Predicting GPS Fidelity in Heavily Forested Areas

Andrew Moore
Dynamic Systems and Controls Branch
NASA Langley Research Center
Hampton, Virginia USA
andrew.j.moore@nasa.gov

Nicholas Rymer
National Institute of Aerospace
Hampton, Virginia USA

J. Sloan Glover
Analytical Mechanics Associates
Hampton, Virginia USA

Derin Ozturk
School of Electrical and Computer Engineering
Cornell University
Ithaca NY USA

Abstract—**There is a compelling need to advance the safety of low altitude flight in forested areas. Signal scattering by trees can interfere with GNSS signal reception and can cause navigation loss within and adjacent to woodlands. An estimate of the signal loss vs. foliage depth is needed to quantify navigational degradation by trees at low altitudes. A previous report described a method which attempts to quantify satellite signal degradation caused by foliage by comparing carrier-to-noise ratio (C/N0) to foliage depth along geometric rays cast from the receiver location to the orbital position of GNSS satellites through a 3D matrix of terrain data. A characteristic curve of attenuation vs. foliage depth was found for both L1 and L2 signals at a single forested site. The current study replicates this result at three additional sites, describes refinements to the method, and explores inherent uncertainties that arise from radiofrequency fading and from receiver limitations for weak signals. For the sites surveyed, 60% and 90% of navigational signal is lost at 10m and 20m of foliage depth, respectively. Since this technique uses low-cost hardware and readily available data collection software, it can allow aviators to estimate GNSS position fidelity in flight ranges near trees.**

Keywords—GPS, GLONASS, GNSS degradation, multilateration, fading, attenuation, foliage, UAV, UAS, lidar, voxel

I. INTRODUCTION

Navigation by means of Global Positioning System (GPS) satellites is readily available in areas free of tall structures and heavy foliage. However, at low altitudes amidst buildings and trees, satellite signals are blocked and attenuated, and position calculations can be degraded or lost entirely. Since unmanned aerial vehicles and urban mobility aircraft routinely make use of satellite-based navigation, including at sites near tall structures and foliage, such degradation or loss can be catastrophic.

Prediction of navigational loss or degradation at low altitudes requires rich 3D terrain data and computational geometry calculations to determine blockage between orbital satellites and the target geography. In the past, researchers have used optical methods at a very few geolocations to estimate terrain elements that could interfere with satellite reception [1][2][3]. The increasing availability of 3D terrain lidar allows estimation GNSS signal obstruction at low altitude with levels of accuracy previously unobtainable, and recently a class of methods emerged which attempt to make such predictions, albeit with simplified physics [4][5][6]. Even in their current form these methods are useful in navigation, since they can rapidly reveal which satellites signals are available for position calculation and which may be blocked or degraded by foliage in the signal path. However, an estimate of the variation in signal loss with foliage depth is needed to quantify navigational degradation by foliage.

This paper describes new results of a previously reported method [7] that attempted to quantify satellite signal degradation caused by foliage. The method compares signal strength to foliage depth along geometric rays cast from the receiver location to the orbital position of GPS satellites through a 3D matrix of obstructions derived from aerial lidar survey data.

II. OBJECTIVES

Three objectives were pursued in the reported work:

a) Validation of GPS signal attenuation vs. canopy depth
b) Refinement of measurement technique: fixing receiver position
c) Refinement of computation technique: preprocess and exclude building lidar

A. Validation of GPS signal attenuation vs. canopy depth

The previous results [7] revealed a characteristic curve of attenuation vs. foliage depth, analogous to that found in radio frequency foliage attenuation studies compiled by the International Telecommunications Union [8]. The attenuation curve was consistent across multiple measurements (55 recordings over two years) at one forested site. Measurements at other sites are needed to show that the attenuation curve found at the original site is not merely an artifact of the methodology.

This paper reports on measurement and analysis at three additional sites. The species mix of trees at two of these sites is similar to the original site. The third site is within a grove of mostly one species. The characteristic curve result found in [7] is replicated at all three sites as described in *Results* below. The radio principles that underlie the curve and the curve limitations at high canopy depth are examined in the *Discussion* section.

B. Refinement of measurement technique: fixing receiver position

Since measurements are by necessity carried out in heavily wooded sites subject to GPS degradation, the ground truth receiver position as computed by multilateration can shift and drift markedly over time. In the previous study, GPS signal measurements were collected via receivers carried and flown into a heavily wooded area along a fixed heading, starting from a location with unobstructed GPS reception. These measurement recording durations were brief, on the order of one minute. The

XXX-X-XXXX-XXXX-X/XX/$XX.00 ©20XX IEEE

receiver rig was equipped with inertial measurement unit (IMU) hardware and a barometric pressure altimeter. Because the initial position was known and stable (in the unobstructed launch area), and because the straight-line trajectory posed a relatively well-bounded position change during the brief recordings, a reasonable ground truth position could be estimated by mixing the GPS, altimeter and IMU data streams with a Kalman filter.

In the current study, experiments with the receiver moving along a varied-heading trajectory (for example, L-shaped) were attempted but abandoned. Even with altimeter and IMU supplements to GPS readings, the estimated position of the roving receiver was markedly unstable. Estimated lateral position deviation was especially severe and could not be used reliably as the ground truth origin in a raycasting calculation.

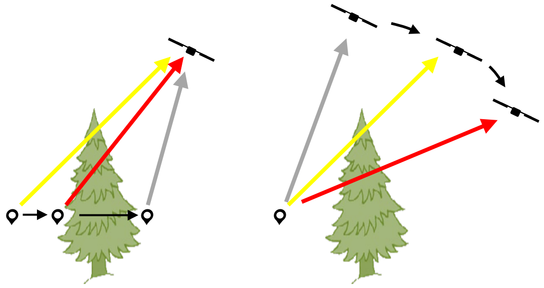

Fig. 1. Moving vs. stationary recording. Left: A moving rover samples the canopy along a ray to a relatively motionless satellite, and in this example records a slightly attenuated signal (yellow ray), then a highly attenuated signal (red ray) and then an unobstructed signal (grey ray). Right: A stationary receiver relies on orbital position changes of the broadcasting satellite, recording an unobstructed signal, then a slightly attenuated signal, then a highly attenuated signal.

As an alternative, long-duration stationary recordings with a fixed ground truth position were collected. The experimental cost of changing from a moving to fixed rover is significant – the recording times must be much longer to effectively sample the nearby canopy. In brief moving-rover measurements, satellite positions are essentially fixed (Fig. 1, left). Each ray from the rover to a satellite sweeps through the terrain canopy as the ray's origin moves, and in a minute or so, much of the canopy is sampled by the rover-to-orbit rays. In contrast, if the receiver is fixed on the ground (Fig. 1, right), the rover-to-orbit rays change only slowly as the satellite position changes – roughly 30° per hour.

C. *Refinement of computation technique: preprocess and exclude building lidar*

In the measurement site studies in [7], there were few buildings, and canopy depth was computed using only a foliage lidar array derived from an aerial lidar survey dataset. A second derived lidar array of buildings was utilized in this study, constructed to enable exclusion of canopy depth calculation along rays that intersect buildings. In particular, a) building lidar was preprocessed to add points to building interiors, and b) building lidar was organized into an array of 3D voxels designated differently (by numerical density values) than foliage voxels. The array construction and raycasting through the tree canopy are described in the *Methodology* section below.

III. METHODOLOGY

A. *Lidar and site description*

An aerial lidar survey of the NASA Langley Research Center collected on March 28, 2018 was used to construct terrain data at four measurement sites: a) a steam pipeline corridor abutted by tree (Pipeline site), b) a parking lot wooded on three sides (Wythe Creek site), c) a treelined walkway between two buildings separated by ~ 45m (West Reid site), and d) a tree stump in deep woods (Shepard site).

Sites. The four sites are indicated on the overview map shown in Fig. 2. Closeups of each site are shown in Fig. 3. Site conditions are as follows: a) Pipeline, a 70m section of cleared corridor 10m-20m in width, containing a steam pipeline and gravel path abutted by 200m of dense forest, b) Wythe Creek, a 30x30m^2 gravel parking lot framed on the north by a single story building, on the west and south by 100m of forest, and on the east by 200m of forest; c) West Reid, a sidewalk between two buildings separated by 45m, bordered by two rows of tall sycamore (*Platanus occidentalis*) and shorter crape myrtle (*Lagerstroemia speciosa*) trees, and d) Shepard, a tree stump completely surrounded by dense forest (radial enclosure from 70m to 250m). The forest at the Pipeline, West Reid and Shepard sites are composed of a variety of native species indigenous to the Hampton Roads area of Virginia including sweetgum (*Liquidambar styraciflua*), sycamore, red maple (*Acer rubrum*), hickory (*Carya speciosa*), loblolly pine (*Pinus taeda*) and eastern red cedar (*Juniperus virginiana*).

Ground truth position. At the Pipeline site, a location outside the forest with stable GPS position served as the as the launch site for flights and starting point of ground level (walking) GPS signal collection. Flight paths at 5m and 40m altitude above ground are shown in Fig. 4. Post-processing of GPS signals with RTKLIB (version 2.4.3/demo5/b31 [9]) could not produce a stable and reasonable set of points along a linear path from the clear aunch area to a point 70m deep in the woods. However, the Ardupilot™,[1] ArduCopter (v3.5.3) autopilot software was able to combine the GPS position data and readings from the inertial sensors and barometric altimeter on the measurement rig (i.e., on the Pixhawk™ autopilot) to yield a series of ground truth points that agreed reasonably well to the known longitude, latitude, and altitude of the measurement line. The measurement line is shown in yellow in Fig. 3. At the other sites, aerial maps were used to select ground positions that were distinct and geolocatable (red markers in three rightmost images in Fig. 3), because GPS receiver lock was poor or completely lost.

Lidar preparation. The average point spacing of the lidar dataset was 10cm. It was processed for raycasting in four steps. First, ground points were removed (cutoff: 5m MSL, ~2m AGL). Second, to aid in separation of the lidar dataset into building and tree point cloud arrays, an intermediate 2D GIS

---

[1] The use of trademarks or names of manufacturers in this report is for accurate reporting and does not constitute an official endorsement, either expressed or implied, of such products or manufacturers by the National Aeronautics and Space Administration.

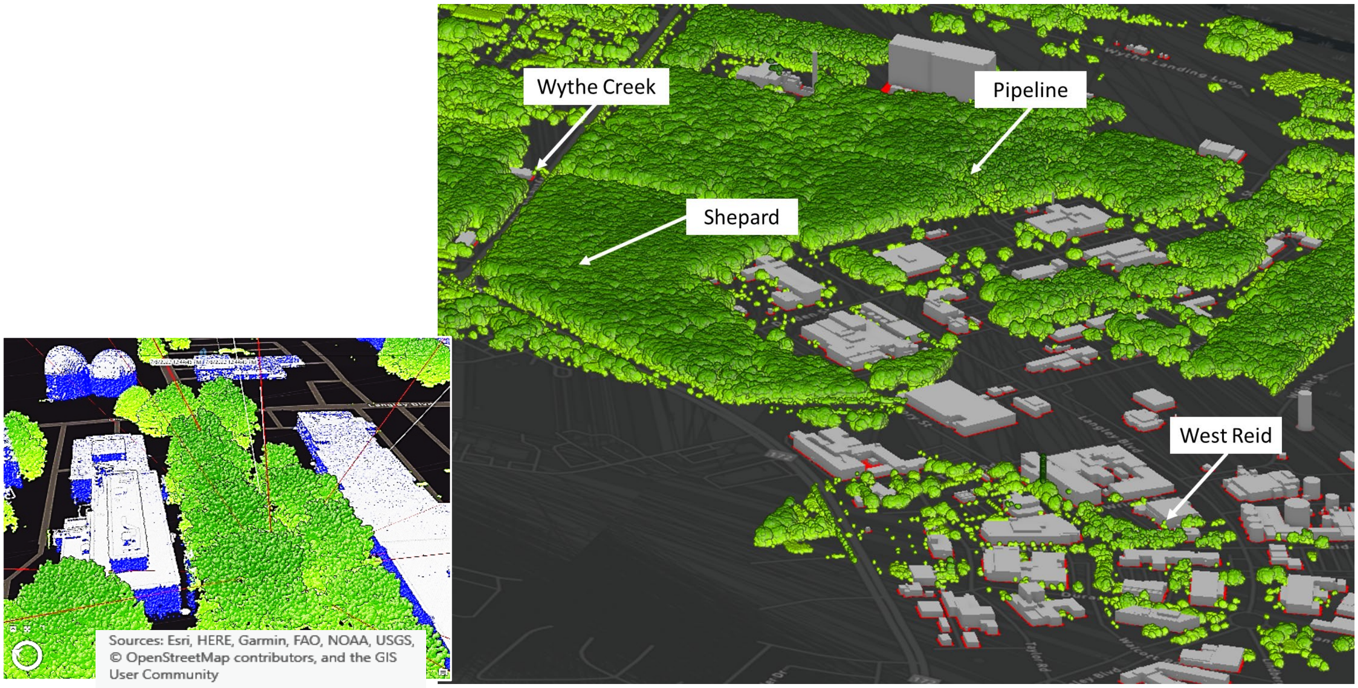

Fig. 2. Geodata of measurement sites. Foreground: Lidar of foliage (green) and buildings (grey) with vertical fill (blue) at one instant of measurement at the West Reid site. Rays to satellites are shown as red if obstruction is found and grey is there is a clear line of sight to the satellite. Background: View of all measurement sites with foliage lidar (green) and building shapefiles (grey) atop spatial expansion of building footprints (red) used to separate foliage and building point clouds.

Fig. 3. Foliage attenuation measurement sites, from left to right: Pipeline, Wythe Creek, West Reid and Shepard. Measurements were taken along a line at this Pipeline site (yellow) and at fixed locations at the other sites (red markers). Map data ©2023 Google, Landsat/Copernicus, SIO, NOAA, U.S.Navy, NGA, GEBCO, Terrametrics, USGS

layer was created by expanding building footprints outward by 3m (red features in Fig. 2) Third, all lidar points inside this intermediate layer were saved to a building lidar array, and all lidar points outside it were saved to a tree lidar array. Fourth, lidar points were added to fill the interior volume of buildings at 0.5m steps in altitude from the rooftop to ground (blue dots in inset of Fig. 2).

B. *Raycasting*

The computation of ray obstruction is similar to volume raycasting in computer graphics [10] and computed tomography [11]. In volume raycasting, paths from a viewpoint to points on the volume boundary are found, and points of intersection with objects along each path are accumulated to estimate object transparency. This is less computationally demanding than raytracing [12], in which ray reflections from object surfaces are also considered. Reflections of orbital global navigation satellite system (GNSS) signals from the terrain (called multipath signals [13][14]) are not computed in this method.

Rays projected from the georeferenced receiver position to the satellite positions may intersect with buildings, foliage, or both. To obtain attenuation values that result only from foliage obstruction, rays that intersect a building at any point must be excluded from the computation. Aerial lidar surveys often cannot sample the sides of buildings faithfully. The near-vertical angle of the downward-pointing laser may only graze the side of a building, and a building side may be shadowed by the building roof. To aid in excluding rays that intersect buildings, lidar was preprocessed to fill the interior of buildings by adding solid points at 0.5m steps in altitude from the rooftop to ground. (See inset of Fig. 2 for an example.) Since a 0.5m voxel size was used to construct the spatial octree of the lidar, this guaranteed that any ray intersection with a building was detectable.

Foliage and building lidar, organized as two spatially aligned point clouds f and b, were loaded into Point Cloud Library (PCL, [15]) and collected into 3D octree voxel arrays V_f and V_b with a voxel size of 0.5 m^3. Each octree was comprised only of occupied voxels, i.e., a voxel was created in the octree only if its volume enclosed one or more lidar points. (See [7] for further lidar collection details and an image of a resultant octree.)

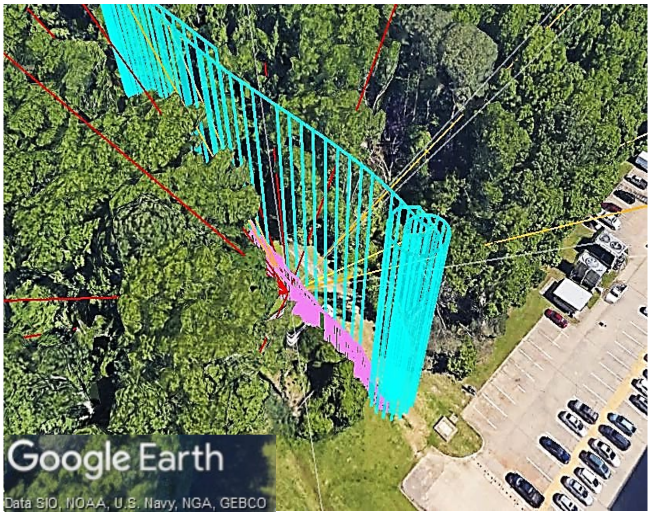

Fig. 4. Flight range in arboreal canyon at the Pipeline site. Trajectory of 40m (cyan) and 5m (pink) flights on 12/14/2018 with rays cast to orbital satellites at one time instant of the 5m flight. The ray color varies from grey (unobstructed) to yellow (obstruction 0.5m to 4.5m) to red (obstruction 5m or more) . ©Map data: Google, NASA

The set of n rays $\overrightarrow{LH}$ was constructed at each recording time t, originating from a low-altitude ground truth point L to high-altitude points H (the orbital position of each of n satellites above horizon at time t). GPS and Global'naya Navigatsionnaya Sputnikovaya Sistema (GLONASS) GNSS constellation orbital positions were obtained from NASA's Archive of Space Geodesy Data [16]. For each of the n rays $\overrightarrow{LH}$ at time t, a C++ program using the PCL library (version 1.7.2) of point cloud functions found all voxels $V_{LH,i}$ intersected by the ray in either array, V_f or V_b . Voxel occupancy values were assigned to allow rejection of buildings and accumulation of canopy depth as follows (equations 1 and 2).

- The voxels of the building array V_b were assigned a voxel occupancy value of 1, and if ray $V_{LH,i}$ intersected any voxel with density 1, the ray was removed from further consideration.
- The voxels of the foliage array V_f were assigned a voxel occupancy value of 0.5, to match the voxel side length. Since the foliage voxel occupancy value equals its linear dimension, this value can be interpreted as linear density, i.e., amount of foliage per unit length. The traversal length δ through each foliage voxel was computed by comparing the ray angle and the normal vector of the intersected voxel face ($\delta = 0.5 * \sqrt{3}$ for a ray that traversed the diagonal of the cubic volume, $\delta = 0.5$ for a ray with a 90° angle to a voxel face, $\delta < 0.5$ for a ray that
- Traversal lengths along each ray were summed to find the total canopy obstruction depth d_{LH} between the receiver and the satellite.

$$\{\forall \overrightarrow{LH}(t) \mid (V_b \cap \overrightarrow{LH}(t)) = 0\}:\ V_{LH,i} = (V_f \cap \overrightarrow{LH}(t)) \quad (1)$$

$$d_{LH} = \sum_i \delta_{f,i} \quad (2)$$

Interior-filling lidar preprocessing for buildings and the array-based ray exclusion (equation 1) was needed to accurately compute canopy depth for a small grove of trees in a walkway between buildings (West Reid site). Canopy depth was computed using only a foliage array for the Pipeline site in the previous study [7] since there are few nearby buildings. The Pipeline site raycasting was recomputed for this report with a building array and compared to the previous foliage-only results; only minor differences were observed.

Raycasting is the most computationally intensive processing step in the method. To compute obstructions for all satellites at each 3600 one second intervals in one hour of stationary recording, about 5 minutes of run time is required on a machine with two 8-core 2.6 GHz Xeon E5-2670 CPUs (32 total threads) and 128GB of RAM. Raycasting for the much smaller number of time steps of a typical flight path (2-4 minutes, or 120-240 one second intervals) at the Pipeline site runs on the same hardware in about 10 seconds.

C. Signal collection and processing

GNSS signals from both US GPS and Russian GLONASS constellations were recorded from two receivers: a) L1 signals from a u-blox^{TM} NEO-M8T attached to a commodity patch antenna (Onshine ANT-555) and b) L1 and L2 signals from a u-blox ZED-F9P ('zed9') integrated with a low profile patch antenna on a 40mm x 47mm ground plane.

Data collection at the Pipeline site was described previously [7]. At the Wythe Creek site, both stationary and moving recordings were collected. For moving recordings, the receivers were carried along the borders of the site on paths of varied heading (for example, L-shaped). Raycasting at points along the movement path was attempted but abandoned - even with barometric and inertial supplements to GPS estimates, the reported receiver position uncertainty during moving intervals was severe and could not be used reliably as the ground truth origin in a raycasting calculation. Moving recordings from the Wythe Creek site were not processed further. Only stationary measurement data was collected and used to compute foliage attenuation at the West Reid and Shepard sites. For stationary recordings, the receivers were placed at a location with a clear georeference confirmed with satellite imagery and georeferenced lidar, which was used as the ground truth location for raycasting. Table 1 summarizes the recording locations, dates, and measurement method (moving or fixed/stationary).

Post processing of the sensor data with RTKLIB and custom bash and Python scripts yielded time-stamped satellite signal carrier-to-noise ratio (C/N0) values. These were matched with the computed foliage depth according to the timestamp and satellite ID using Pandas [17] and plotted with matplotlib [18].

TABLE 1. DATA COLLECTED AT MEASUREMENT SITES

	Pipeline	**Wythe Creek**	**West Reid**	**Shepard**
# Recordings L1/L2	48/7	4/0	12/6	6/3
Dates	2018/11/02 through 2021/02/10 See [7]	2020/10/27 2020/11/18	2022/06/30 2022/07/08 2022/07/12	2022/08/24
Moving/fixed	Both	Fixed	Fixed	Fixed

IV. RESULTS

Receiver signal (C/N0) vs. canopy depth for the four measurement sites are plotted in Fig. 5 (blue dots). At left are L1 signal results, and at right are L2 signal results (except for the Wythe Creek site, due to invalid L2 recordings). All signal recordings from all measurement sets of a particular site are combined in these plots, e.g., for the West Reid site, twelve L1 recordings and six L2 recordings are combined. Plots for individual measurement sets are consistent with these combined results as previously observed in [7] and in the example shown for the Shepard site in Fig. 6.

A characteristic curve (black line) of the form

$$A_f = A_m \, [\, 1 - exp\,(-\, d\,\gamma \,/\, A_m)\,] \tag{3}$$

is overlaid on all L1 results, and a second curve of the same form is overlaid on the L2 results. In this relation, A_f is the attenuation by foliage at canopy depth d, A_m is the maximum attenuation, and γ is the incremental path attenuation. Coefficients for the L1 and L2 curves were chosen to fit the Pipeline site results and are shown in Table 2. Continuous wave radio (CWR) studies [8] shows that maximum attenuation increases with frequency; as expected, A_m is higher in the L1 band (GPS: 1575.42 MHz; GLONASS: 1602.0–1615.5 MHz) than the L2 band (GPS: 1227.60 MHz; GLONASS: 1246.0–1256.5 MHz).

TABLE 2. COEFFICIENTS OF NOMINAL CHARACTERISTIC CURVES

Signal/Coefficient	**A_m (dB-Hz)**	**γ (dB/m)**
L1	35	0.315
L2	30	0.246

The curves chosen reasonably fit the Pipeline and Shepard results. The fit is less good for the Wythe Creek results; a higher maximum attenuation A_m would fit better. Since the canopy depth at the West Reid site is low (≤15m) compared to other sites, there is no data for the higher depths expected to produce maximum attenuation. Further, the rise rate of the fitted curve rise (described via the incremental path attenuation γ), seems low for the West Reid measurements. Since there are only sycamore and crape myrtle trees at the West Reid site, this may be evidence for the species-specific attenuation seen in CWR studies [8].

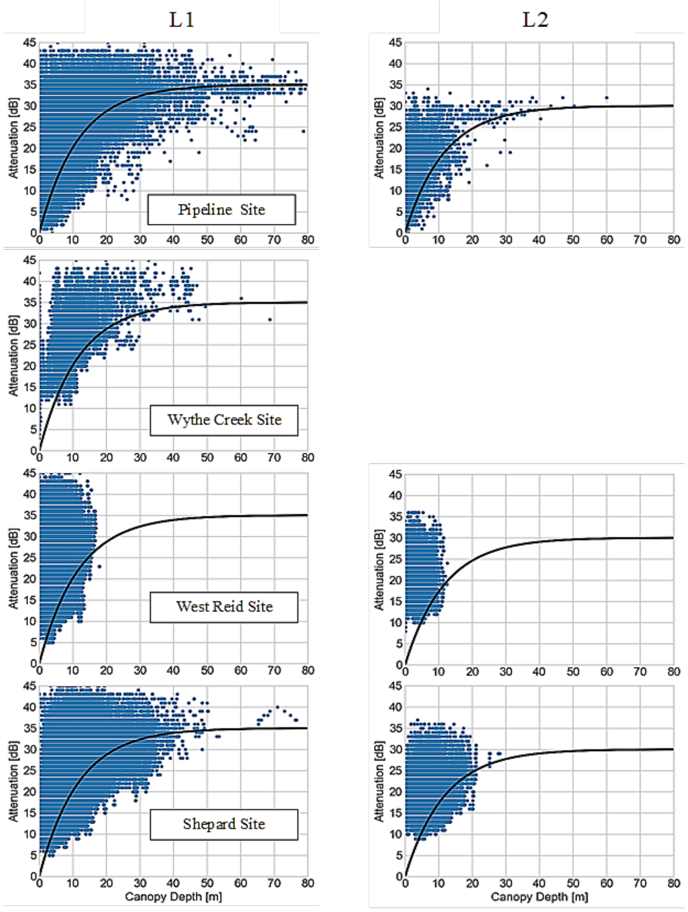

Fig. 5. Receiver signal (C/N0) vs. foliage depth for the four measurement sites. Left: L1 signal results. Right: L2 signal results. L2 recordings at the Wythe Creek site were invalid and are not shown. For both L1 and L2 results, an illustrative characteristic curve that reasonably fits the Pipeline results is overlaid on results for all sites (black lines).

The plots in Fig. 5 exhibit pronounced noise along the y-axis, such that multiple C/N0 values are commonly measured for a given canopy thickness. (One explanation for this is described in the next section.) Because of this, there was no attempt to numerically find the best fit curve, and the particular curves shown in Fig. 5, while reasonable, should be regarded as notional and illustrative.

V. DISCUSSION

A. *Scattering artifacts and noise in the characteristic curve*

A parametric fit to the attenuation vs. opacity curve is inexact, due to a spread in recorded attenuation values for a given canopy depth value. Examination of the signals that comprise the excess attenuation curve shows that this likely arises from signal fading due to scattering effects (Fig. 6).

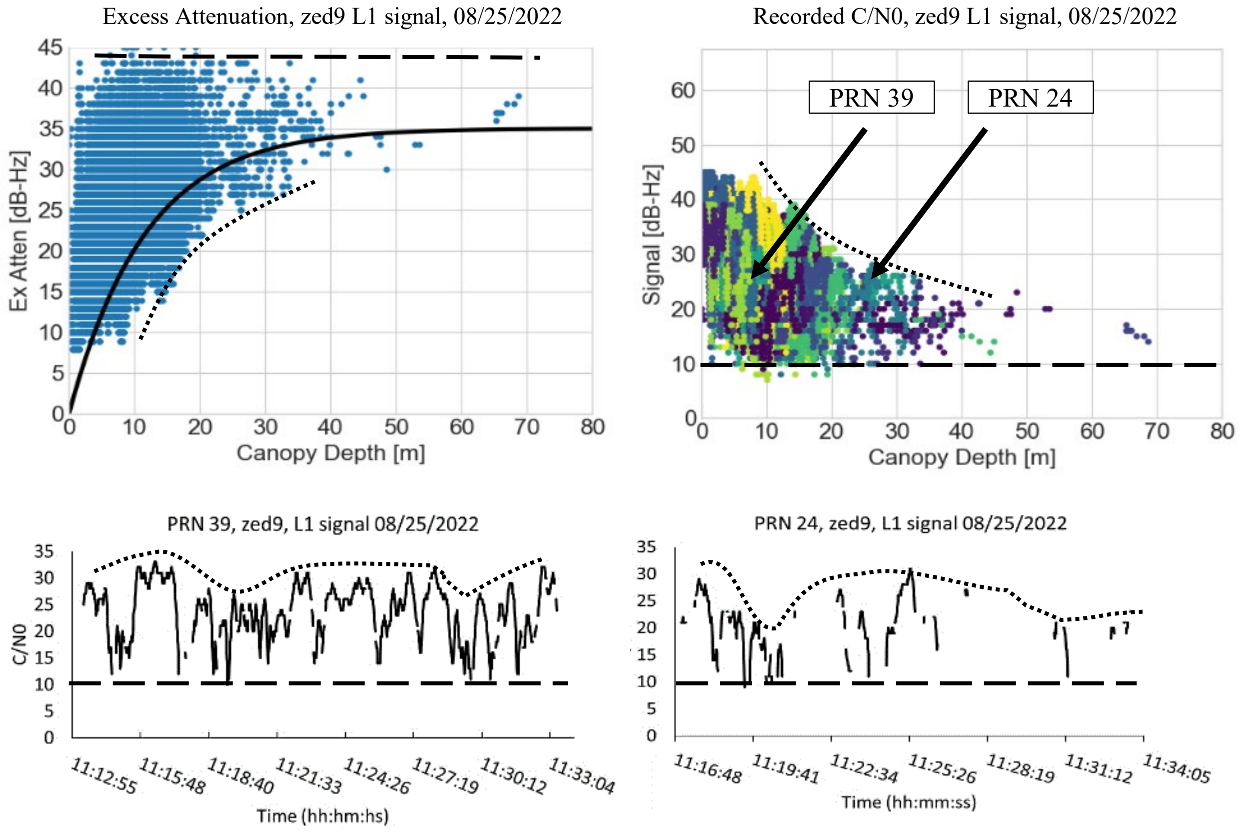

Fig. 6. Multiple C/N0 readings per depth are explained by scattering effects. Top left: L1 signal attenuation vs. depth measurements (blue dots) at Shepard site, 08/25/2022 for zed9 sensor. An estimated characteristic curve is superimposed in solid black. The bottom dotted curve tracks the positive peaks of the signal range, and the top dashed curve tracks the negative peaks and/or the detection minimum. Top right: raw C/N0 values, colored by satellite. The values for PRN 39 (GLONASS #7, light green dots) and PRN 24 (US GPS #24, blue dots) are indicated by arrows and plotted below. Note that the absolute minimum value possible with this sensor is 10 dB-Hz (dashed line). Bottom left: time series of C/N0 from PRN 39. Though the canopy depth changes modestly during this 20-minute interval, the signal fades over range of about 20 dB-Hz, indicating scattering effects. Bottom right: deeper in the forest, the signal from PRN 24 shows frequent dropout, and while the positive peaks of the faded signal are evident, most negative peaks drop below the detection minimum.

A radio receiver subjected to increasing signal shadowing – from clear, unobstructed line-of-sight reception to complete line-of-sight blockage – must contend with increasing signal degradation as the transmitted component is distorted by scattered components [19][20]. Scattered components combine in vector (phasor) summation with the line-of-sight component, and if the transmitter or receiver is moving, the vector sum changes with time and the received signal varies in amplitude (fades) through cycles of constructive and destructive interference [21][22](see [23] for examples of GPS fading). If the line-of-sight signal power is high relative to the scattered power (Rician fading), the minimum received amplitude stays above zero or fades to zero only occasionally. As shadowing is increased to the point that only scattered power is reaching the receiver, complete signal dropout can occur frequently (Rayleigh fading [24][25]).

The signal phenomena that result in a GNSS foliage attenuation curve are shown in Fig. 6. At top left, an excess attenuation curve (black solid line) is overlaid on measured C/N0 values plotted against computed canopy depth (blue dots). Multiple C/N0 values are found for a given canopy depth, with the incidence of multiple values more common for low depth values than high depth values. The greater range of values at low canopy depth might be interpreted as a sign of greater uncertainty in measurement; in fact, there is more uncertainty at *high* canopy depths, as revealed by examination of the time series of satellite (or space vehicle, SV) readings at different depths. At top right, the measurements are plotted according to the exponential operand of equation (3),

$$s = s_{max} * exp\,(-\,k_2 d\,) \tag{4}$$

where s is the signal, s_{max} is the unattenuated (clear sky) signal strength, and d is canopy depth. Here, C/N0 values are colored the same for each measured SV and the receiver minimum signal level (10 dB-Hz) is shown as a dashed line. Two series of illustrative SV signals (PRN 39 and PRN 24, black arrows) are plotted at bottom. The PRN 39signal, obstructed by ~10m of canopy, shows periodic deep fading as the SV moves through the sky (bottom left of Fig. 6). At a given canopy depth, signal values are recorded over the entire amplitude range from the peak to the trough of the faded signal. The PRN 39 signal series is consistent with Rician fading, as the trough values remain above zero. The PRN 24 signal, obstructed by ~20m of canopy, shows fading at about the same periodicity, and fades to an undetectable level (at or below 10 dB-Hz) much of the time. Whether the trough values drop to zero (consistent with Rayleigh scattering) is impossible to know due to the receiver threshold cutoff at the 10 dB-Hz detection minimum.

Low signal levels near the detection minimum are unavailable for the autocorrelation processing that is central to GPS signal amplification and SV identification. Signal levels at or near the radio detection minimum cannot be separated from background noise and cannot be recorded. Thus, deep in the canopy, received carrier-to-noise values depth values are measurable over a small range due to truncation of the faded signal. The impression of greater certainty at high canopy depth is thus an artifact of the nature of GPS reception: the lower C/N0 range at high canopy depth only indicates that signals are near the extremes of detection.

The bounds of spread of C/N0 values at a particular depth on the characteristic curve (top left of Fig. 6) can then be understood as ranging from a 'ceiling' (dashed line) corresponding to the receiver low-signal cutoff and a 'floor' (dotted line) corresponding to peak of the faded signal.

Which of the range of values between the fading-driven floor and ceiling levels should be used to find the 'true' attenuation value? *In situ* GNSS measurements cannot answer that question because to eliminate fading the relative transmitter-receiver movement must be halted and that is not possible with GNSS satellites. This is a research area that could be addressed by 1) a reference transmitter or 2) an enhanced receiver. An example of (1) is a terrestrial transmitter of known power broadcasting a simulated GNSS signal (similar to a pseudolite [26]). Readings of the received power variation with distance and canopy depth could be used to calibrate the receiver. An example of (2) is a customized antenna/receiver system that senses signal polarization (see [27] for example). This would allow separation of those scattered signals which have also reflected (and thereby changed polarization).

Until these or other efforts are applied to narrow the faded GNSS receiver signal range, foliage attenuation curves must be approximated.

B. *Models of foliage attenuation*

Full integro-differential propagation (i.e., radiative transfer) modelling [28] may be needed to fully capture the complex interactions of microwave radio signals with foliage. There are distinct disadvantages to using radiative transfer modeling. It requires rich, precise terrain data, its output can vary significantly with small input geometry errors, it is sensitive to boundary conditions, and it is computationally intensive.

In this and the prior study, we use a 2nd order approximation of CWR signal attenuation with canopy depth of the form adopted by the International Telecommunications Union [8]. In extensive measurement campaigns a decade and more ago, investigators measured CWR foliage attenuation in varied tree species, foliage state (in-leaf or out-of-leaf), and grove geometry, and proposed various models to fit the results. Equation (3) and other 2nd order approximations were fitted to data collected at gigahertz radio frequencies (see for example [28][29][30]). There is not a consensus in the literature about which of the several proposed second-order function best describes the observed CWR effects. The candidate functions can all closely fit observed data at low foliage depths, but their predictions diverge for high canopy depths — some predict a flat saturation level, while others predict a linear or power-law rise (top of Fig. 7). Due to the signal fading and dropout described above and in Fig. 6, any proposed function that performs well at low canopy depth is sufficient, since high-depth measurements are not reliable (shaded area at bottom of Fig. 7).

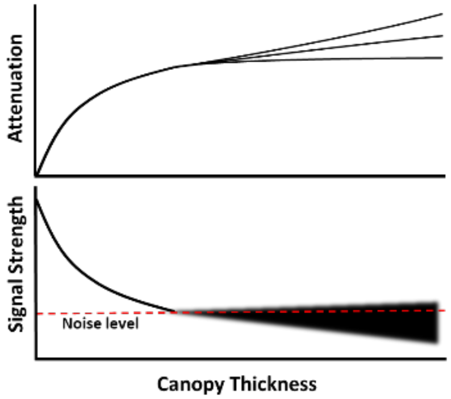

Fig. 7. Top: Second-order CWR model variation at high canopy depth. Bottom: GNSS carrier to noise ratio *vs.* canopy depth and minimum resolvable signal strength (dashed line).

C. *Recommendations for navigation*

Navigational impairment in foliage may be intermittent or persistent.

Intermittent. Two of the authors conducted a series of flight experiments to explore the feasibility of UAV-based inspection of high voltage transmission lines [31][32]. This type of infrastructure is often located adjacent to forests and in deep arboreal canyons, away from buildings, and we occasionally faced unexplained, intermittent navigational loss for intervals of 5-10 minutes. The current investigation into GNSS impairment by foliage was motivated by that experience, as a way to mitigate — or at least explain — the navigational safety risk endemic to low-altitude flight near trees.

We have not found a means to mitigate intermittent navigation loss near trees that is compact and lightweight enough to fly on a small UAV. The results of this study do help explain positional intermittency, however, and suggest an operational principle. Signals scattered from foliage can combine at the receiver to produce Rician fading of the sort illustrated in Fig. 6. The geometry of the GNSS constellation, treeline, and flight path can, on occasion and for short time intervals, result in deep fading of enough satellite signals to lose navigational lock. If so, then navigation should be re-established after waiting a few minutes for the position of the GNSS satellites to change, as we observed in the transmission line flight campaign.

Persistent. At the sites studied, we find that ~60% of GNSS signal strength is lost at 10m of canopy depth, and ~90% of signal strength is lost at 20m of canopy depth for both L1 and

L2 GNSS signals (Fig. 5). The persistent navigation uncertainty 10-20m deep in a forest can be expected to be accompanied by intermittent loss of all GNSS navigation.

D. Limitations

Limitations of this survey method were enumerated in [7] and are reiterated here in approximate order from most to least severe:

1. Ground truth positional error
2. Physics simplification 1: Raycast only; no reflection, diffraction or multipath
3. Antenna sensitivity vs. elevation assumed uniform
4. Voxel quantization error
5. Physics simplification 2: Season disregarded, in-leaf and out-of-leaf treated the same
6. Positional error in lidar

We found limitation (1) the most vexing at first, when using moving-rover recordings. This limitation was nearly eliminated by shifting to stationary geolocated measurements. Fast multipath geometry computation (i.e., raytracing as opposed to raycasting) would remove limitation (2), but the added computational cost may be considerable. Efforts to overcome this technology limitation are especially needed to compute signal reflections in urban areas [33], near treelines, and in arboreal canyons. Typical antenna sensitivity variations are low (e.g., 7-10 dB) relative to the variation caused by fading. For the Pipeline site recordings, we attempted to address limitation (3) using recorded UAV roll and pitch, but found no discernible benefit. Voxel size was varied over a wide range (from 0.1m^3 to 10m^3) to assess limitation (4). Quantization artifacts in attenuation vs. density plots were evident at voxel sizes of 5m^3 and higher. Voxel dimensions lower than the 0.5m^3 used throughout this study added some fine structure in attenuation vs. density plots but this had no analytical benefit, i.e., the upper and lower bounds of the C/N0 points for a given canopy depth did not change appreciably. We found no benefit in separating attenuation analysis by time of year to assess limitation (5). For some species, modest (20%) seasonal variation of incremental path attenuation is observed in CWR studies [8], but this was not evident in cross-seasonal comparisons of Pipeline site measurements. Since a single lidar set from an in-leaf date (March 28, 2018) was used for raycasting, no seasonal density change can be expected; the strong signal variation caused by fading may mask seasonal signal variation. Comparison of the lidar point cloud to other, independent map data, showed that the positional error of the lidar used in this study (limitation 6) is occasionally up to 2m but typically less than 1m.

As discussed in depth above, we would add two more limitations:

7. Imprecise signal strength due to signal fading
8. Receiver-dependent detection threshold

In our judgement these limitations should be ranked between (2) and (3), i.e., less severe than the raycast sufficiency assumption and far more severe than the antenna uniformity assumption. It is straightforward to fit a characteristic curve within the ‘cloud’ of signal values caused by limitation (7) and positioned well below the ceiling imposed by limitation (8) as in Fig. 5 and Fig. 6. The navigational recommendations discussed above are not appreciably altered by minor curve fitting adjustments.

VI. CONCLUSIONS

The oft-held assumption that GNSS navigation is reliable at locations away from buildings is only partially true. Navigation loss can occur when signals are scattered by tree canopies and interfere with broadcast GNSS signals.

A novel method to quantify foliage attenuation of GPS signals was applied at four heavily wooded sites. As long as measurement data from a reliably located position is used and signal paths that intersect building are excluded, results from the technique are consistent across sites. While the output of method is noisy due to radio limitations inherent in GNSS receivers, it can be readily fit with a standard continuous wave radio curve to yield practical navigation guidelines. For the mix of species surveyed, navigation is persistently impaired at short (~10m) distances inside of forests and the risk of total navigation loss is high when surrounded by trees by 20m or more.

There is a compelling need to advance the safety of low altitude flight in forested areas [34]. Currently there exist few studies of foliage impacts on the on GNSS navigation fidelity, and with the method described more species and sites could be surveyed at low cost.

VII. ACKNOWLEDGEMENTS

We are grateful to the many NASA Langley Research Center colleagues for discussions and assistance in the course of this multi-year development effort: Scott Dorsey, Evan Dill and Steve Young (GNSS); Russell Gilabert (RTKLIB); Robert Gage and J. Berch Smithson (lidar and coordinate systems); Mark Frye and Daniel Healey of the UAS Operations Office, under the leadership of Tom Jordan, served as Range Safety Officers; Christina Guldin advised on safety matters; and Kyle Ellis and Misty Davies for program support. D. Ozturk acknowledges the University Space Research Association for internship logistics. This work was performed with support from the NASA Unmanned Traffic Management program and System Wide Safety Project, which is part of NASA's Aviation Operations and Safety Program. J. Berch Smithson of the Midland GSS Joint Venture provided lidar surveys of the NASA Langley Research Center.

VIII. REFERENCES

[1] Wright, W.C. Quantifying Global Position System Signal Attenuation as a Function of Three-Dimensional Forest Canopy Structure; University of Florida: Gainesville, FL, USA, 2008.

[2] Wright, W., Wilkinson, B. and Cropper Jr, W., 2018. Development of a GPS forest signal absorption coefficient index. Forests, 9(5), p.226.

[3] Holden, N.M., Martin, A.A., Owende, P.M.O. and Ward, S.M., 2001. A method for relating GPS performance to forest canopy. International Journal of Forest Engineering, 12(2), pp.51-56.

[4] E. Dill, J. Gutierrez, S. Young, A. Moore, A. Sholz, E. Bates, K. Schmitt, J. Doughty, “A predictive GNSS Performance Monitor for Autonomous Air Vehicles in Urban Environments”, Institute of Navigation (ION) Global Navigation Satellite Systems (GNSS+) Conference, September 2021.

[5] F. van Diggelen, “End Game for Urban GNSS: Google’s Use of 3D Building Models,” Inside GNSS, March/April 2021, Vol. 16(2), pp. 42-49, 2021.

[6] Bennett, N., Hunter, M., & Buesnel, G. (2021). Validation of urban multipath models with record and playback simulation. In Proceedings of the 34th international technical meeting of the satellite division of the institute of navigation (ion gnss+ 2021).

[7] Moore, A., Schubert, M., Rymer, N., Villalobos, D., Glover, J., Ozturk, D., & Dill, E. (2022). Volume raycasting of GNSS signals through ground structure lidar for UAV navigational guidance and safety estimation. AIAA Scitech 2022 Forum. 2022.

[8] Attenuation in Vegetation ITU-R Recommendation P833-10, Geneva, September 2021.

[9] Everett, T., rtklibexplorer, RTKLIB Demo5, 2021 URL: https://github.com/rinex20/RTKLIB-demo5

[10] Roth, Scott D. "Ray casting for modeling solids." Computer graphics and image processing 18, no. 2 (1982): 109-144.

[11] Wang, Sidney W., and Arie E. Kaufman. "Volume-sampled 3D modeling." IEEE Computer Graphics and Applications 14, no. 5 (1994): 26-32.

[12] Cook, Robert L., Thomas Porter, and Loren Carpenter. "Distributed ray tracing." In ACM SIGGRAPH computer graphics, vol. 18, no. 3, pp. 137-145. ACM, 1984.

[13] Ray, Jayanta Kumar, and M. Elizabeth Cannon. "Characterization of GPS carrier phase multipath." In Proceedings of ION National Technical Meeting, pp. 243-252. 1999.

[14] Panicciari, Tommaso, Soliman, Mohamed Ali, Moura, Grégory, "Evaluation of a GNSS Receiver Performance in Different Multipath Environments with a Novel Real-time Multipath Simulation System," Proceedings of the 30th International Technical Meeting of The Satellite Division of the Institute of Navigation (ION GNSS+ 2017), Portland, Oregon, September 2017, pp. 427-435.

[15] Rusu, Radu Bogdan, and Steve Cousins. "3d is here: Point cloud library (pcl)." In 2011 IEEE international conference on robotics and automation, pp. 1-4. IEEE, 2011.

[16] Crustal Dynamics Data Information System, https://cddis.nasa.gov/

[17] McKinney, W., 2011. pandas: a foundational Python library for data analysis and statistics. Python for high performance and scientific computing, 14(9), pp.1-9.

[18] Hunter, J.D., 2007. Matplotlib: A 2D graphics environment. Computing in science & engineering, 9(03), pp.90-95.

[19] Braasch, M.S. and Van Dierendonck, A.J., 1999. GPS receiver architectures and measurements. Proceedings of the IEEE, 87(1), pp.48-64.

[20] Schubert, F.M., Fleury, B.H., Robertson, P., Prieto-Cerdeirai, R., Steingass, A. and Lehner, A., 2010, April. Modeling of multipath propagation components caused by trees and forests. In Proceedings of the Fourth European Conference on Antennas and Propagation (pp. 1-5). IEEE.

[21] Al-Nuaimi, M.O. and Stephens, R.B.L., 1998. Measurements and prediction model optimisation for signal attenuation in vegetation media at centimetre wave frequencies. IEE Proceedings-Microwaves, Antennas and Propagation, 145(3), pp.201-206.

[22] Goldhirsh, Julius, and Wolfhard J. Vogel. "Handbook of propagation effects for vehicular and personal mobile satellite systems." NASA Reference Publication 1274 (1998): 40-67.

[23] Kumar, G. , Rao, G. and Kumar, M. (2013) GPS Signal Short-Term Propagation Characteristics Modeling in Urban Areas for Precise Navigation Applications. Positioning, 4, 192-199. doi: 10.4236/pos.2013.42019.

[24] International Telecommunications Union, Probability distributions relevant to radiowave propagation modelling ITU-R Recommendation P.1057-4, Geneva, September 2015.

[25] Ma, C., Jee, G.I., MacGougan, G., Lachapelle, G., Bloebaum, S., Cox, G., Garin, L. and Shewfelt, J., 2001, September. Gps signal degradation modeling. In Proceedings of the 14th International Technical Meeting of the Satellite Division of the Institute of Navigation (ION GPS 2001) (pp. 882-893).

[26] Dai, L., Zhang, J., Rizos, C., Han, S. and Wang, J., 2000, September. GPS and pseudolite integration for deformation monitoring applications. In Proceedings of the 13th International Technical Meeting of the Satellite Division of the Institute of Navigation (ION GPS 2000) (pp. 1-8).

[27] Lau, L. and Cross, P., 2007. Development and testing of a new ray-tracing approach to GNSS carrier-phase multipath modelling. Journal of Geodesy, 81, pp.713-732.

[28] Adegoke AS. Measurement of propagation loss in trees at SHF frequencies, PhD Thesis, University of Leicester, United Kingdom; 2014

[29] Savage, N., Ndzi, D., Seville, A., Vilar, E. and Austin, J., 2003. Radio wave propagation through vegetation: Factors influencing signal attenuation. Radio Science, 38(5), pp.9-1.

[30] Rogers, N.C., Seville, A., Richter, J., Ndzi, D., Savage, N., Caldeirinha, R., Shukla, A.K., Al-Nuaimi, M.O., Craig, K., Vilar, E. and Austin, J., 2002. A generic model of 1-60 GHz radio propagation through vegetation-final report. Radio Agency, UK, 152, p.152.

[31] Moore, Andrew, Matthew Schubert, and Nicholas Rymer. "Autonomous Inspection of Electrical Transmission Structures with Airborne UV Sensors and Automated Air Traffic Management." In 2018 AIAA Information Systems-AIAA Infotech@ Aerospace, p. 1628. 2018.

[32] Moore, Andrew J., Matthew Schubert, Nicholas Rymer, Swee Balachandran, Maria Consiglio, Cesar Munoz, Joshua Smith, Dexter Lewis, and Paul Schneider. "UAV Inspection of Electrical Transmission Infrastructure with Path Conformance Autonomy and Lidar-based Geofences NASA Report on UTM Reference Mission Flights at Southern Company Flights November 2016." NASA Technical Memo (2017): 2017-219673.

[33] Accuracy Assessment of Two GPS Fidelity Prediction Services in Urban Terrain, Andrew Moore, Julian Gutierrez, Evan Dill, Michael Logan, J. Sloan Glover, Steven Young, Nathan Hoege, 2023 IEEE/ION Position, Location and Navigation Symposium (PLANS), Monterey, CA, 2023

[34] S. Young, E. Ancel, A. Moore, E. Dill, C. Quach, J. Foster, K. Darafsheh, K. Smalling, S. Vazquez, E. Evans et al., “Architecture and information requirements to assess and predict flight safety risks during highly autonomous urban flight operations,” NASA Tech Memo NASA-TM-2020-220440. 2020.